 doi.org/10.52568/001421/JCSP/46.01.2024

Green Synthesis, Characterization and Thermal Investigation of Ni(II) and Cu(II) Complexes Constructed by Pyridine-2,6-Dicarboxylic Acid

Xi Jiang, Zhao-Hui Chen, Huan Luo, Rong-Gui Yang, Ting Liu and Guo-Qing Zhong*
[1]*School of Materials and Chemistry, Southwest University of Science and Technology, Mianyang 621010, Sichuan, P. R. China.*
[2]*School of Chemistry and Chemical Engineering, Southwest University, Chongqing 400715, P. R. China.*
zgq316@163.com*

(Received on 18th March 2022, accepted in revised form 23rd June 2023)

Summary: Two complexes $[Ni(pda)(H_2pda)]\cdot 3H_2O$ (**1**) and $[Cu(pda)(H_2pda)]$ (**2**) containing pyridine-2,6-dicarboxylic acid (H_2pda) were synthesized by room-temperature solid state reaction and characterized by elemental analyses, powder X-ray diffraction (PXRD), single crystal X-ray diffraction and infrared spectroscopy. The powder complexes were confirmed as single phase with their PXRD. The thermal property was studied using simultaneous thermogravimetry and differential scanning calorimetry (TG-DSC) techniques. The complexes were decomposed in several stages and the final products of their thermal decomposition were NiO and CuO, respectively. In order to explore application of the complexes, the nano-NiO and nano-CuO particles were produced by using the powder complexes as precursors at different temperatures. The particles were characterized and observed by PXRD and scanning electron microscope (SEM), and their average diameters of the pyrolysis products at 500 ℃ were about 12 and 30 nm, respectively.

Keywords: Pyridine-2,6-dicarboxylic acid; Ni(II) and Cu(II) complexes; Thermal decomposition; Nano oxide; X-ray diffraction.

Introduction

Pyridine-2,6-dicarboxylic acid (H_2pda) contains one pyridine ring and two carboxyl groups, it has attracted much interest in the synthesis of compounds for its novel topologies and interesting structural motifs to construct supermolecule architectures [1], MOFs [2, 3], coordination polymers [4, 5] and two-dimensional and three-dimensional networks [6, 7]. Stereochemistry [8], luminescence property [9], magnetism [10, 11], spectroscopy [12], reaction dynamics [13] and diversified biological activity [14–18] of its derivatives and complexes had been deeply and widely studied. Nickel and copper are the essential trace elements for life, and their organic acid complexes are widely present in the living body for their special biological activities and catalytic effects on the life system [19, 20]. Moreover, the theoretical and application studies of their complexes for organic carboxylic acids are emerging [21–25].

The Ni(II) and Cu(II) complexes of H_2pda were reported in many literatures [26–30]. However, these complexes were almost synthesized by liquid phase method, which has the disadvantages of complicated operation, high energy consumption and serious environmental pollution. In this paper, the Ni(II) and Cu(II) complexes of H_2pda ($[Ni(pda)(H_2pda)]\cdot 3H_2O$ (**1**) and $[Cu(pda)(H_2pda)]$ (**2**)) were synthesized by solid state reaction at room-temperature [31]. Comparing with liquid phase method, such method is in accord with the conception of green chemistry and makes up for the shortcomings of liquid phase synthesis. Then their single crystals were successfully cultured by the solvent evaporation method using the powder complexes, which confirmed that the powder complexes obtained from solid state reaction at room-temperature was pure phase. There are two ligand molecules in the title complexes, one of which removes all protons and the other retains all protons. And the crystal structure analysis indicates that the complexes are different from the reported structural parameters and crystallographic data [32, 33]. The main difference of the Ni(II) complex is the deprotonization degree of the ligand, and the main differences of the Cu(II) complex are the diversity of crystal water, crystal system and space group.

NiO, a P-type semiconductor material with good chemical stability and electrical properties, is widely used in the fields of catalysis and composite ceramics [34]. CuO, a kind of antimagnetic P-type semiconductor functional material with unique physical and chemical properties such as photoconductivity, field emission effect, catalytic and electrode activity, is widely used in the fields of field effect tubes, electrochemistry, gas sensors, etc [35]. In order to explore application of the title complexes, the NiO and CuO particles with high purity and small particle size were obtained by calcination with their

*To whom all correspondence should be addressed.

powder complexes as precursors. Moreover, the particle size of oxides, which has a great influence on property and application, can be controlled by adjusting the thermal decomposition temperature within a certain temperature range. Many methods for preparing nano-NiO and nano-CuO have been reported such as precipitation [36], electrodeposition [37, 38], sol-gel [39] and microemulsion method [40]. However, this thermal decomposition method, which uses the powder complexes obtained from solid state reaction at room-temperature as precursors, is one of the more advantageous methods for simple preparation process and low cost.

Experimental

Materials and instruments

Pyridine-2,6-dicarboxylic acid (H_2pda) was obtained from Jinan Henghua Sci. & Tec. Co., Ltd., while $Cu(Ac)_2{\cdot}H_2O$, $Ni(Ac)_2{\cdot}4H_2O$ and ethanol was purchased from Tianjin Guangfu Fine Chemical Research Institution. All chemical reagents purchased were of analytical pure and without further purification.

The C, H and N analyses were performed on an Elementar Vario EL CUBE instrument. The contents of Ni and Cu in the complexes or oxides were determined by the EDTA titration. The PXRD patterns were obtained by a Rigaku D/max-II X-ray diffractometer using Cu *K*α radiation. Fourier transform infrared spectra (FT-IR) were measured with potassium bromide pellets in the range of 4000–400 cm^{-1} on a Nicolet iS50 FT-IR spectrometer. Thermogravimetry and differential scanning calorimetry analyses (TG and DSC) were performed by a SDT Q650 thermal analyzer and the measurements were recorded from ambient temperature to 800 °C at a heating rate of 10 °C min^{-1} under a nitrogen flow of 100 mL min^{-1}. Single crystal structure determination was performed with a Bruker SMART APEX II CCD diffractometer equipped with a graphite-monochro-matized Mo *K*α radiation (λ = 0.71073 Å). SEM images were measured on a Tescan MAIA3 field emission scanning electron microscope system.

Synthesis of [Ni(pda)(H_2pda)]·3H_2O (**1**)

H_2pda (0.668 g, 4.00 mmol) and $Ni(Ac)_2{\cdot}4H_2O$ (0.498 g, 2.00 mmol) were mixed and carefully ground in an agate mortar, and two drops of ethanol were added as initiator. The irritative acetic acid gas was released during the grinding process, indicating that the reaction did happen. No irritant produced after about 4 h of grinding, and the product (it was directly prepared by room-temperature solid state reaction without separation and purification, and it called the powder complex in this paper) was green powder and its PXRD pattern was determined. Subsequently, the powder was dissolved with a suitable amount of distilled water, and the filtered liquor was heated and concentrated to about 30 mL. The green crystals of [Ni(pda)(H_2pda)]·3H_2O (**1**) in about 71% (based on H_2pda) were generated after 10 days. Anal Calc. (Found, %) for $NiC_{14}H_{14}O_{11}N_2$ (**1**): C 37.79 (38.01), H 3.17 (3.30), N 6.30 (6.16) and Ni 13.19 (13.13). FT-IR (KBr, cm^{-1}): 3391(s), 3099(w), 1594(s), 1446(m), 1382(m), 769(s), 723(m), 549(m), 436(s).

Synthesis of [Cu(pda)(H_2pda)] (**2**)

The reactants of H_2pda (0.668 g, 4.00 mmol) and $Cu(Ac)_2{\cdot}H_2O$ (0.399 g, 2.00 mmol) were mixed up well together. The synthetic method of **2** was similar to that of **1**. The product obtained was blue powder and its PXRD pattern was determined. Subsequently, the blue crystals of [Cu(pda)(H_2pda)] (**2**) in about 64% (based on H_2pda) were generated after 14 days. Anal Calc. (Found, %) for $CuC_{14}H_8O_8N_2$ **(2)**: C 42.49 (42.10), H 2.04 (2.16), N 7.08 (7.17.) and Cu 16.06 (16.21). FT-IR (KBr, cm^{-1}): 3409(s), 3102(w), 1622(s), 1380(w), 1348(w), 594(m), 444(m).

Preparation of nano-NiO and nano-CuO

The powder complexes **1** and **2** were calcined in a KSL-100X muffle furnace at 400, 500, 600 and 800 °C for 0.5 h, respectively, under an air atmosphere. The nano-NiO and nano-CuO with a narrow-size distribution were generated. The effect of calcination temperature on the particle size of nano-NiO and nano-CuO was investigated.

X-ray crystallography

The single crystal of [Ni(pda)(H_2pda)]·3H_2O (**1**) or [Cu(pda)(H_2pda)] (**2**) was selected and fixed with epoxy cement on fine glass fibers, which was then mounted on a Bruker SMART APEX II CCD diffractometer with graphite-monochromated Mo Kα radiation (λ = 0.71073 Å). The structure was solved with the SHELXS-97 program and refined on F^2 by using SHELXL-97 program [41]. All nonhydrogen atoms were refined anisotropically and hydrogen atom positions were refined in isotropic approximation using a riding model. The crystal data and structure parameters of the complexes are summarized in Table-1, and the selected bond lengths and angles are listed in Table-2. CCDC numbers are 1921383 for **1** and 1921384 for **2**, and these data can be obtained free of charge *via* http://www.ccdc.cam.ac.uk/conts/retrieving.html.

Table-1: Crystal data and structure refinement parameters for **1** and **2**.

Complex	1	2
Empirical formula	$NiC_{14}H_{14}O_{11}N_2$	$CuC_{14}H_8O_8N_2$
Formula weight (g·mol^{-1})	444.98	395.76
Temperature (K)	293(2)	293(2)
Crystal system	Monoclinic	Monoclinic
Space group	$P2_1/c$	$P2_1/c$
a (Å)	13.6696(5)	13.4230(7)
b (Å)	10.0440(4)	10.3112(5)
c (Å)	13.7673(5)	13.8035(7)
β (°)	115.1670(10)	114.260(2)
V (Å^3)	1710.78(11)	1741.79(15)
Z	4	4
Calculated density (g·cm^{-3})	1.728	1.509
Absorption coefficient (mm^{-1})	1.201	1.296
F(000)	912	796
Crystal size (mm)	0.25 × 0.21 × 0.17	0.36 × 0.32 × 0.26
Theta range (°)	2.970 to 27.544	2.970 to 27.524
Limiting indices	$-17\le h\le 17$, $-13\le k\le 13$, $-17\le l\le 17$	$-17\le h\le 17$, $-13\le k\le 13$, $-17\le l\le 17$
Reflections collected / unique	26196 / 3925 (R_{int} = 0.0270)	26601 / 3992 (R_{int} = 0.0231)
Completeness to theta = 25.242	99.9%	99.6%
Max. and min. transmission	0.7456 and 0.5991	0.7456 and 0.5597
Data / restraints / parameters	3925 / 9 / 263	3992 / 48 / 226
Goodness-of-fit on F^2	1.085	1.006
Final R indices [$I>2\sigma(I)$]	R_1 = 0.0453, wR_2 = 0.1263	R_1 = 0.1629, wR_2 = 0.4182
R indices (all data)	R_1 = 0.0545, wR_2 = 0.1335	R_1 = 0.1656, wR_2 = 0.4193
Largest diff. peak and hole (e·Å^{-3})	0.374 and –1.171	1.357 and –1.922

Table-2: Selected bond distances (Å) and angles (°) for **1** and **2**.

Complex 1		Complex 2	
Ni1—O1	2.1699(17)	Cu1—O1	2.201(11)
Ni1—O3	2.0953(18)	Cu1—O3	2.170(10)
Ni1—O5	2.1954(18)	Cu1—O5	2.234(15)
Ni1—O7	2.0997(18)	Cu1—O7	2.157(9)
Ni1—N1	1.9606(19)	Cu1—N1	1.951(9)
Ni1—N2	1.9662(19)	Cu1—N2	1.949(9)
N2—Ni1—O7	78.59(8)	O3—Cu1—O5	93.8(4)
O1—Ni1—O5	91.39(7)	O3—Cu1—O1	154.4(4)
O3—Ni1—O5	93.21(7)	N1—Cu1—O3	76.7(4)
O3—Ni1—O1	155.92(7)	N1—Cu1—O7	103.2(4)
O3—Ni1—O7	92.85(7)	N1—Cu1—O5	101.5(4)
O7—Ni1—O5	155.09(7)	N1—Cu1—O1	77.8(4)
O7—Ni1—O1	92.86(8)	O7—Cu1—O3	93.0(4)
N1—Ni1—O5	104.37(7)	O7—Cu1—O5	155.3(4)
N1—Ni1—O1	77.14(7)	O7—Cu1—O1	92.8(4)
N1—Ni1—O3	78.82(7)	N2—Cu1—O3	103.8(4)
N1—Ni1—O7	100.51(8)	N2—Cu1—N1	179.5(4)
N1—Ni1—N2	176.32(8)	N2—Cu1—O7	77.0(4)
N2—Ni1—O5	76.50(8)	N2—Cu1—O5	78.2(4)
N2—Ni1—O1	99.30(7)	N2—Cu1—O1	101.8(4)
N2—Ni1—O3	104.76(7)	O1—Cu1—O5	91.3(4)

Table-3: Parameters of hydrogen bonds for **1** and **2**.

Complex	D—H···A	d(D—H) (Å)	d(H···A) (Å)	d(D···A) (Å)	∠(DHA) (°)
1	O9—H9A···O2	0.85	1.62	2.4634(1)	171.0
	O9—H9B···O11	0.85	1.71	2.5135(1)	156.0
	O10—H10A···O6	0.85	1.67	2.4750(1)	157.0
	O10—H10B···O4	0.85	1.94	2.7432(1)	157.0
	O11—H11A···O1	0.85	2.22	2.7790(1)	123.0
	O11—H11B···O8	0.85	2.08	2.6006(1)	119.0
	C3—H3···O5	0.93	2.52	3.2018(1)	130.0
	C12—H12···O3)	0.93	2.55	3.2728(1)	135.0
2	C5—H5···O7	0.93	2.48	3.2089(2)	136.0
	C10—H10···O1	0.93	2.44	3.1943(2)	138.0

Results and discussion

Description of the structure

Description of [Ni(pda)(H_2pda)]·3H_2O (**1**). The asymmetric unit of **1** contains one Ni(II) center, one pyridine-2,6-dicarboxylic acid molecule (H_2pda) (which contains O1, O3 and N1), one pyridine-2,6-dicarboxylate dianions (pda^{2-}) (which contains O5, O7 and N2) and three crystal water molecules (Fig. 1). The bond angles (N1—Ni1—O3 78.82°, N1—Ni1—O1 77.14°, N2—Ni1—O1 99.30° and N2—Ni1—O3 104.76°] add up to 360.02°, so the O1, N1, O3, N2 and Ni1 atoms are almost in the same plane. The geometry around Ni(II) can be described as a slightly distorted octahedron with the O1 and O3 atoms of H_2pda and the N1 and N2 atoms

building the equatorial plane and the O5 and O7 atoms of pda^{2-} occupying the axial positions. Hydrogen bonds of **1** are listed in Table-3, and the extensive hydrogen bonds are formed through the interactions of O atoms from carboxyl groups and free crystal water molecules, which result in a 3D network (Fig. 2).

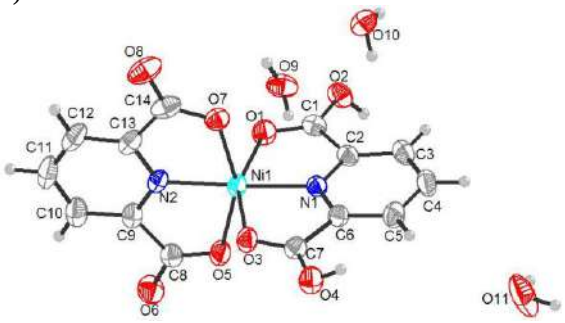

Fig. 1: Molecular structure of **1**.

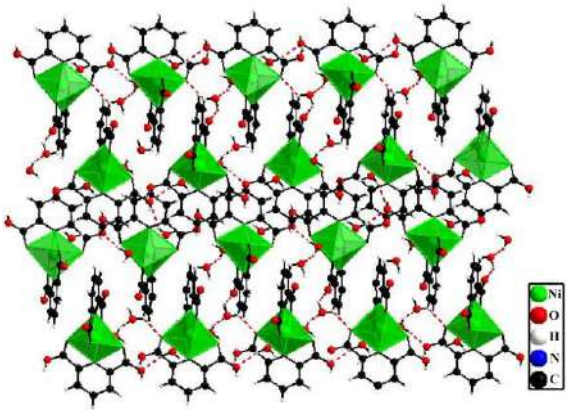

Fig. 2: 3D network structure of **1**.

Description of [Cu(pda)(H_2pda)] (**2**). The asymmetric unit of **2** consists of one Cu(II) center, one pyridine-2,6-dicarboxylate molecule (H_2pda) and one pyridine-2,6-dicarboxylate dianions (pda^{2-}) (Fig. 3). Average value 2.186 Å of Cu1—O1 (2.201 Å) and Cu1—O3 (2.170 Å) is very close to that 2.196 Å of Cu1—O5 (2.234 Å) and Cu1—O7 (2.157 Å), so the O1, O3, O5 and O7 atoms are almost in the same plane. Average value of Cu1—N1 (1.951 Å) and Cu1—N2 (1.949 Å) is 1.950 Å, and the average value is shorter than that of Cu—O bonds due to Jahn-Teller effect. Thus, the geometry around Cu(II) ion can be described as an axially compressed octahedron with the O1, O3, O5 and O7 atoms building equatorial plane, and the N1 and N2 atoms occupying axial positions (Fig. 3). Hydrogen bonds of **2** are given in Table-3 and the 3D spatial network structure is formed by weak hydrogen bonds (C5—H5···O7 and C10—H10···O1) between molecules (Fig. 4).

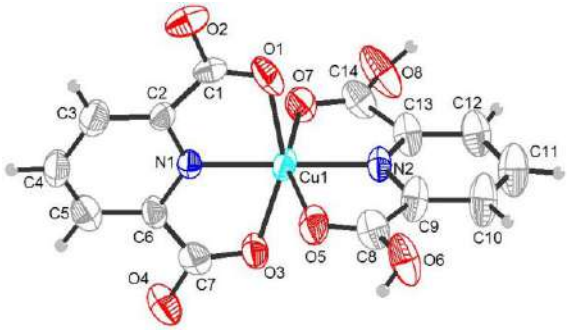

Fig. 3: Molecular structure of **2**.

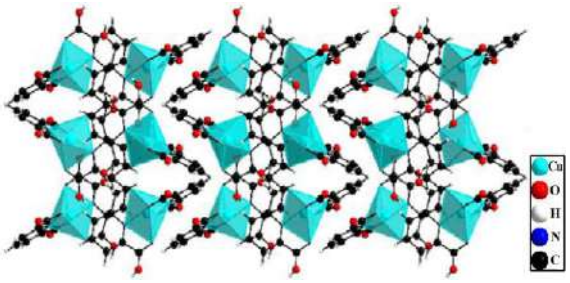

Fig. 4: 3D network structure of **2**.

PXRD analysis

In order to verify the formation of **1**, the powder complex obtained by solid state reaction was measured by powder X-ray diffraction. The strong intensity of the diffraction peak indicates a good crystalline state of **1**. The three strong peaks of the powder sample appear at 2θ = 11.63°, 21.33° and 27.51° (Fig. 5b), while the three strong peaks of the crystal sample appear at 11.57°, 21.29° and 27.45° (Fig. 5a), and at 2θ = 27.84°, 16.78° and 19.30° for H_2pda, and at 2θ = 12.88°, 21.03° and 28.30° for nickel acetate (JCPDS No. 25-0901). Comparing with the reactants, the peak locations in PXRD pattern of the powder complex are significantly altered, which confirms the formation of **1** [42]. Subsequently, the powder sample of **1** was dissolved in an appropriate amount of distilled water, and the green crystals were precipitated after 10 days. In order to check the phase purity of the powder complex **1**, the PXRD pattern of its crystal sample is also measured and compared (Fig. 5a). As can be seen from Fig. 5a and Fig. 5b, the positions of their diffraction peaks match well, indicating the consistency of the two samples and the high efficiency of the solid state reaction at room-temperature. Fig. 5c represents the PXRD pattern obtained by simulating diffraction with single crystal diffraction data. Comparing the PXRD patterns of the first two with the simulation result, the diffraction peak positions of the former two are similar to those of the third one, indicating the purity of the sample again.

Table-4: Experimental data and calculated results for PXRD of **1**.

No.	2θ(°)	h	k	l	d_{exp}(Å)	d_{cal}(Å)	I/I_0	No.	2θ(°)	h	k	l	d_{exp}(Å)	d_{cal}(Å)	I/I_0
1	11.63	1	1	–1	7.606	7.604	100.0	29	33.66	2	1	–5	2.660	2.662	2.8
2	12.93	2	0	–1	6.842	6.829	3.5	30	34.30	0	3	–3	2.612	2.613	9.8
3	14.17	0	0	2	6.243	6.247	17.1	31	34.93	5	1	–1	2.566	2.570	2.1
4	14.88	1	1	1	5.948	5.947	17.5	32	35.65	0	4	0	2.516	2.516	1.4
5	15.27	2	0	–2	5.798	5.804	24.9	33	37.08	3	3	1	2.423	2.423	6.1
6	16.82	0	1	2	5.321	5.308	3.6	34	37.90	5	2	–3	2.372	2.374	6.7
7	17.61	0	2	0	5.031	5.032	19.3	35	39.88	5	0	1	2.259	2.256	3.7
8	18.42	1	0	2	4.812	4.816	3.1	36	40.39	1	4	2	2.231	2.230	1.4
9	18.99	0	2	1	4.669	4.668	13.2	37	41.05	4	3	–4	2.197	2.195	4.3
10	20.10	3	0	–2	4.415	4.418	8.1	38	41.74	1	1	–6	2.162	2.161	1.2
11	20.45	1	1	2	4.339	4.344	19.6	39	42.51	4	3	1	2.125	2.126	1.9
12	21.33	0	0	3	4.162	4.165	31.9	40	43.45	0	0	6	2.081	2.082	4.6
13	21.96	3	1	–2	4.045	4.046	16.9	41	44.18	1	4	3	2.048	2.047	2.0
14	22.73	2	2	0	3.909	3.907	16.3	42	44.64	4	3	–5	2.028	2.027	1.6
15	23.13	0	1	3	3.842	3.848	13.1	43	45.76	3	3	3	1.981	1.982	3.0
16	24.16	2	0	2	3.681	3.686	25.5	44	46.99	2	5	–1	1.932	1.931	3.6
17	25.64	2	2	1	3.472	3.473	11.1	45	47.33	7	1	–3	1.919	1.921	2.2
18	25.94	2	0	–4	3.432	3.438	16.8	46	48.59	5	3	1	1.872	1.872	1.4
19	26.41	3	2	–1	3.372	3.371	5.5	47	49.12	4	3	–6	1.852	1.851	1.6
20	26.95	3	1	1	3.306	3.309	1.1	48	49.50	3	5	–1	1.840	1.840	2.7
21	27.51	0	3	–1	3.240	3.240	29.3	49	51.61	0	3	–6	1.770	1.769	1.0
22	27.81	0	2	3	3.206	3.208	6.3	50	52.37	3	5	1	1.746	1.745	1.9
23	28.53	0	0	4	3.126	3.124	2.4	51	54.08	2	4	–6	1.694	1.693	1.1
24	29.22	1	3	1	3.054	3.053	25.6	52	55.32	2	5	3	1.659	1.659	1.6
25	30.12	4	1	0	2.964	2.962	9.9	53	56.83	0	6	–2	1.619	1.620	1.3
26	31.72	4	2	–2	2.819	2.825	3.3	54	62.32	4	6	–3	1.489	1.489	1.4
27	32.05	4	1	–4	2.790	2.789	2.8	55	62.56	6	5	–1	1.484	1.483	1.1
28	32.72	5	0	–2	2.735	2.738	2.7	56	66.52	4	2	6	1.405	1.406	1.3

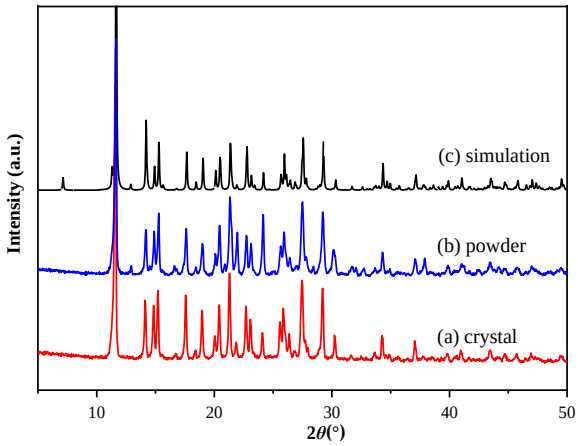

Fig. 5: PXRD patterns of **1**.

The index of PXRD data bases on the computer program [43], and the results for the powder complex **1** are listed in Table-4. All PXRD data of the powder sample can be calculated, and the calculated d_{cal} value is consistent with the experimental d_{exp} value and the largest relative deviation between d_{cal} and d_{exp} is less than 0.3%. As a result, the powder complex prepared is a single phase, its crystal structure belongs to monoclinic system with the cell parameters of a = 13.699 Å, b = 10.064 Å, c = 13.805 Å and β = 115.17°. At the same time, the calculated cell parameters are consistent with the results of single crystal structure analysis and these results can enrich the PXRD database.

The PXRD patterns of the complex **2** is shown in Fig. 6. Comparing with the raw materials, the peak locations of the powder resultant are altered obviously. The strong peaks which come from reactants of H_2pda and copper acetate (JCPDS No. 27-1126) are disappeared in PXRD pattern of the powder product, and this suggests the new compound formation. Then, the powder sample is dissolved in distilled water to grow the single crystal. Blue crystals are precipitated after 14 days. And as can be seen from Fig. 6, the PXRD pattern of the powder sample matches well with that of the single crystal sample and the simulation result.

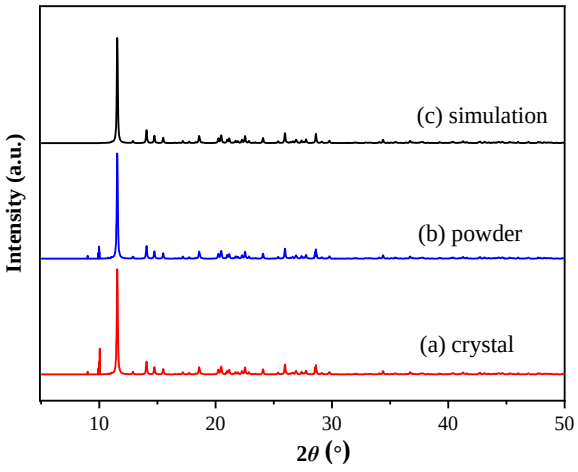

Fig. 6: PXRD patterns of **2**.

Table-5: Thermal decomposition data of **1**.

Possible pyrolytic product	DSC peak (°C)	Mass loss (%)		Assignment
		m_{exp}	m_{cal}	
{Ni[$C_5H_3N(COO)_2C_5H_3N(COOH)_2$]}·3$H_2O$	143 (endo.)	11.63	12.15	Loss of 3H_2O molecules
{Ni[$C_5H_3N(COO)_2C_5H_3N(COOH)_2$]}	277 (exo.)	20.11	19.78	Loss of 2CO_2 molecules
[Ni($C_5H_4NCOO)_2$]	385 (exo.)	52.05	51.28	Dissociation of residual ligand
NiO		16.21	16.79	

FT-IR analysis

Infrared spectra of H_2pda and the complexes are shown in Fig. 7. The strong peak at 1699 cm^{-1} for H_2pda is attributed to that of the free carboxyl group. A strong and wide absorption band appeared near 1600 cm^{-1} for the complexes, indicating that the carboxyl group in the ligand is not completely deprotonated. Comparing with FT-IR spectrum of H_2pda, the peaks at 2625 and 2546 cm^{-1} disappear in **1**, indicating N atom in pyridine ring is coordinated [44]. A wide intense absorption band near 3391 cm^{-1} is determined as the ν(O—H) vibration [31] from crystal water molecules and H_2pda. In Fig. 7b, there is an absorption band at 3099 cm^{-1}, which is assigned to ν(C—H) vibration [45]. The absorption peaks at 1594 and 1382 cm^{-1} are designated as the $\nu_{as}(COO^-)$ and $\nu_s(COO^-)$ vibration, respectively [46]. The difference value $\Delta\nu$ is 212 cm^{-1} and the higher $\Delta\nu$ value compare to Na salt of carboxylate implies the carboxylate groups adopt a monodentate mode coordinated with Ni(II) ion [47-49]. The absorption band at 1446 cm^{-1} is attributed to the ν(C=C) vibration. The absorption peaks at 769 and 723 cm^{-1} are respectively assigned to the rocking and wagging vibrations of hydroxyl group. The absorption peaks at 549 and 436 cm^{-1} are designated to ν(Ni—N) and ν(Ni—O) vibrations, respectively [50].

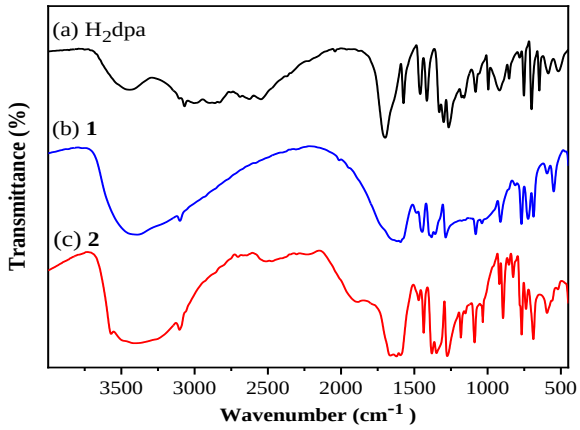

Fig. 7: Infrared spectra of H_2pda, **1** and **2**.

In Fig. 7c, the wide intense absorption of **2** about 3409 cm^{-1} is assigned to the stretching vibration of hydroxyl from H_2pda. The peaks near 1380 and 1348 cm^{-1} are attributed to the $\nu_s(COO^-)$ vibrations, and this group is also reflected in FT-IR spectrum by the $\nu_{as}(COO^-)$ vibration at 1622 cm^{-1}. The higher $\Delta\nu$ value (242 and 274 cm^{-1}) compare to Na salt of carboxylate indicate a monodentate binding of the carboxylate groups to Cu(II) ion [48, 49]. Comparing with infrared spectrum of ligand, the peaks at 2625 and 2546 cm^{-1} disappear in **2**, indicating N atom on the pyridine ring is involved in the coordination. The peak at 1436 cm^{-1} is attributed to the ν(C=C) vibration, and the peaks at 594 and 444 cm^{-1} are designated as the ν(Cu—N) and ν(Cu—O) vibrations, respectively.

Thermal analysis

Thermal analysis of complexes is helpful to understand their stability and coordination structure [51]. The thermal studies of the powder complexes were carried out in the range of 30–800 °C under nitrogen atmosphere. The TG-DSC curves of **1** are depicted in Fig. 8. The first mass loss of 11.63% is close to three crystal water molecules (Calcd. 12.15%), the process is endothermic (DSC maximum at 143 °C), and this confirms the existence of crystalline water molecules. In the second stage, there is an exothermic peak at 277 °C in DSC curve, and 2 mol of CO_2 molecules are removed from the structure with a mass loss of 20.11% (Calcd. 19.78%). The third stage occurs with 52.05% mass loss (Calcd. 51.28%) and it belongs to the oxidative decomposition of 2-pyridine carboxylate ligand. The final residue is NiO with 16.21% (Calcd. 16.79%). The possible thermal decomposition process [52] is shown in Table-5.

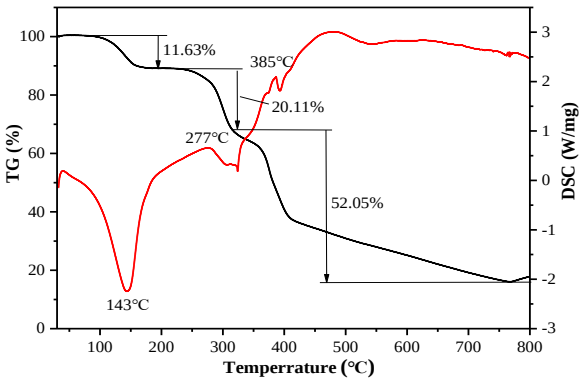

Fig. 8: TG-DSC curves of **1**.

Table-6: Thermal decomposition data of **2**.

Possible pyrolytic product	DSC peak (°C)	Mass loss (%)		Assignment
		m_{exp}	m_{cal}	
{Cu[$C_5H_3N(COO)_2C_5H_3N(COOH)_2$]}	133 (endo.)	11.22	11.12	Loss of CO_2 molecule
{Cu[$C_5H_3N(COO)_2C_5H_4N(COOH)$]}	282 (exo.)	56.91	57.66	Dissociation of residual ligand
$CuCO_3$	290 (endo.)	10.84	11.12	Loss of CO and CO_2 molecules
CuO		21.03	20.10	

The TG-DSC curves of **2** are depicted in Fig. 9. In the first stage, there is an endothermic peak at 133 °C in DSC curve, and 1 mol of CO_2 molecule is removed from the structure with a mass loss of 11.22% (Calcd. 11.12%). The second mass loss corresponding to the exothermic peak at 282 °C is 56.91% (Calcd. 57.66%), 1 mol of H_2O molecule, 2 mol of CO molecules and 2 mol of $–C_5H_3N$ groups are removed from the structure in this stage, and the pyrolysis product is copper carbonate (Found 31.87%, Calcd. 31.22%). The final stage mass loss is 10.84% (Calcd. 11.12%), owing to the release of 1 mol of CO_2 molecule. The final residue is CuO with 21.03% (Calcd. 20.10%). The possible thermal decomposition process is shown in Table-6.

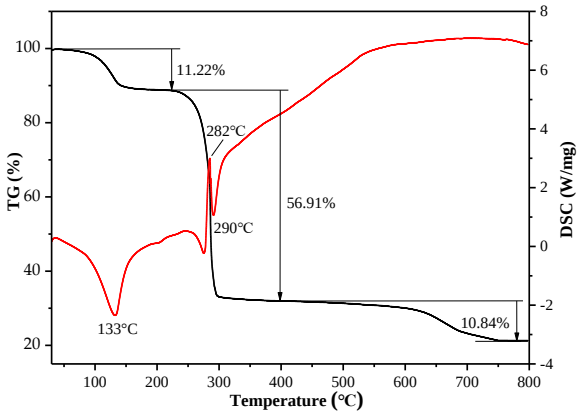

Fig. 9: TG-DSC curves of **2**.

Particle size and morphology of nano-NiO and nano-CuO

The nanometer NiO and CuO were prepared by pyrolysis reaction with the powder complexes **1** and **2** as precursors. The complexes were calcined at 400, 500, 600 and 800 °C for 0.5 h, respectively, and the PXRD patterns of the pyrolysis products are shown in Fig. 10. The main strong peaks of their PXRD patterns are consistent with the standard diffraction card of NiO (JCPDS No. 47-1049) or CuO (JCPDS No. 45-0937). At the same time, the PXRD patterns are also very consistent with that of NiO (A.R.) or CuO (A.R.). As shown in Fig. 10, the diffraction peaks become sharper when the pyrolysis temperature is increased gradually, and this indicates that the particle size of NiO and CuO grows gradually. Calculated by the X-ray single peak Fourier analysis method [53], the average diameters of the NiO at 400, 500, 600 and 800 °C are 7, 10, 14 and 33 nm, and the average diameters of the CuO at 400, 500, 600 and 800 °C are 23, 29, 31 and 37 nm, respectively.

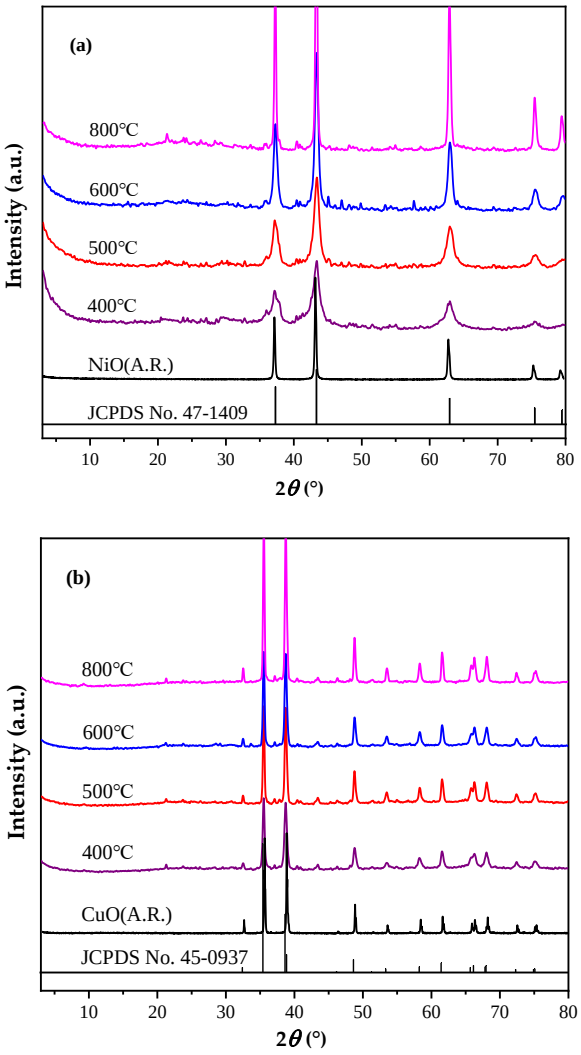

Fig. 10: PXRD patterns obtained by calcination of **1** (a) and **2** (b) at 400, 500, 600 and 800 °C.

Figs. 11 and 12 show the SEM images of the nano-NiO and nano-CuO obtained from calcining **1** and **2** at 500 °C. As can be seen from Figs. 11 and 12, the nano-NiO and nano-CuO particles are almost spherical, and their average particle diameters are

about 12 and 30 nm, which are basically consistent with the PXRD calculation results. Since the dispersion treatment is not performed, the particles are agglomerated together. The content of nano-NiO or nano-CuO is determined by EDTA coordination titration, and the purity of nano-NiO or nano-CuO is high, reaching more than 99.9%. The nano-NiO and nano-CuO prepared by pyrolysis have the advantages of simple operation and uniform particle size. And nano-NiO and nano-CuO of desired particle size can be prepared by controlling calcination temperature. Therefore, the preparation method of the nano-NiO and nano-CuO has popularization and application value.

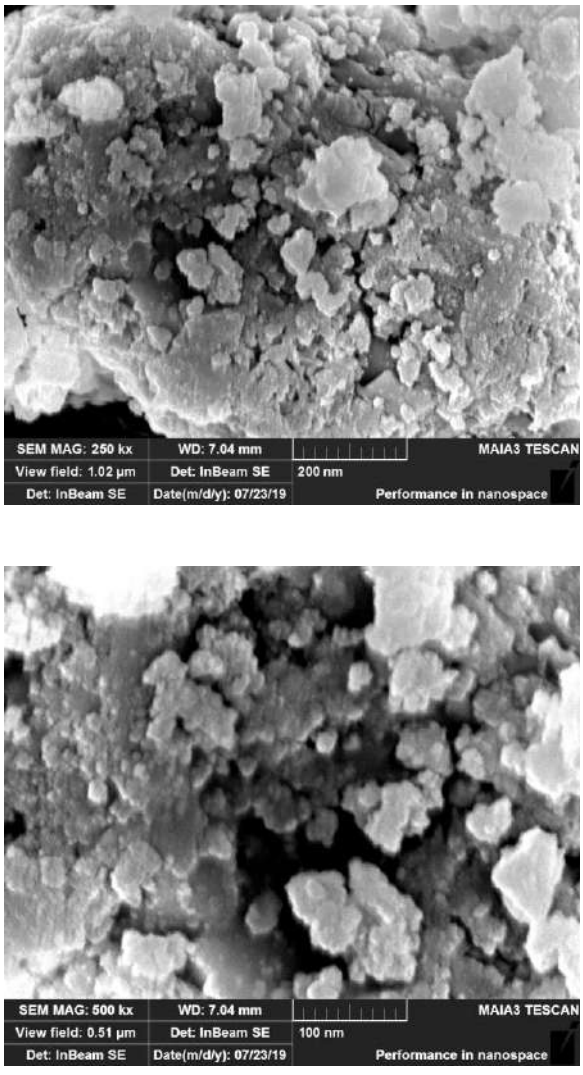

Fig. 11: SEM images of nano-NiO.

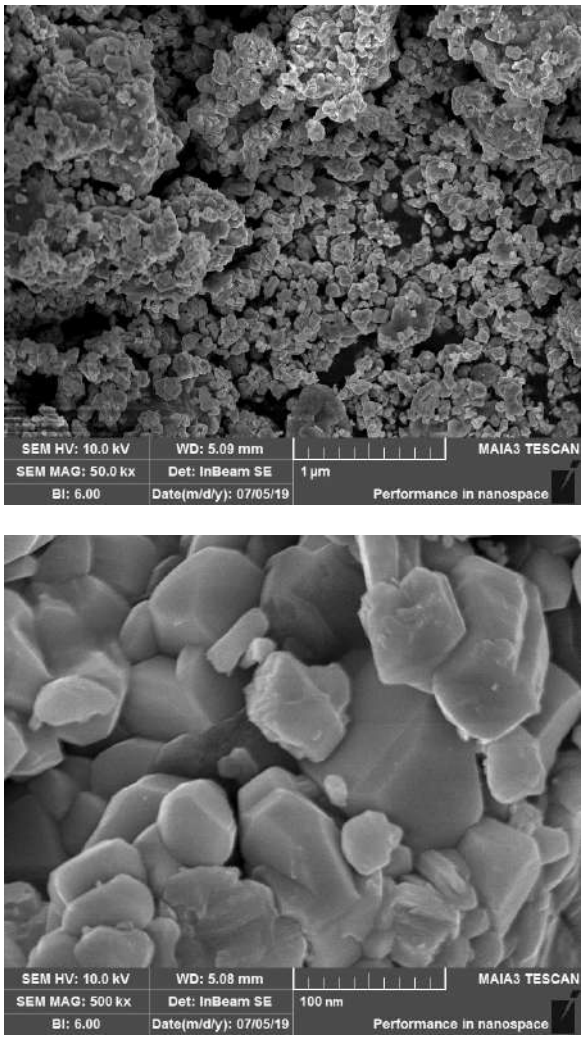

Fig. 12: SEM images of nano-CuO.

Conclusion

The complexes **1** and **2** were synthesized by solid state reaction at room-temperature, and characterized by EA, PXRD, FT-IR and TG-DSC. The powder complexes were confirmed as a single phase from the PXRD results. The crystal structure of the complexes belonged to monoclinic system with $P2_1/c$ space group, and the cell parameters were a = 13.6696(5) Å, b = 10.0440(4) Å, c = 13.7673(5) Å and β = 115.1670(10)° for **1**, and a = 13.4230(7) Å, b = 10.3112(5) Å, c = 13.8035(7) Å and β = 114.260(2)° for **2**. The Ni(II) or Cu(II) ion was hexa-coordinated by four O and two N atoms, and forming a distorted octahedron. The TG-DSC curves of the complexes were mainly due to dehydration, as well as the ligands decarboxylation and oxidative decomposition. The nano-NiO and nano-CuO were prepared by thermal decomposition with their

complexes as precursors, the particle size of NiO and CuO gradually grew with the increase of pyrolysis temperature, and their average diameters of the pyrolysis products at 500 °C are about 12 and 30 nm, respectively. The particles size of NiO and CuO can be changed by controlling the pyrolysis temperature of the precursors. The Ni(II) and Cu(II) complexes of pyridine-2,6-dicarboxylic acid can be synthesized by room-temperature solid state reaction without the need for purification and separation, and the synthesis method has the advantages of simple operation, high yield, energy saving and environmental friendliness.

Acknowledgment

This research was supported by Longshan academic talent research supporting program of SWUST, China (No. 17LZX414).

References

1. L. Han, L. Jin, E. Wang and Z. Su, Synthesis and characterization of two isostructural 3d-4f coordination compounds based on pyridine-2,6-dicarboxylic acid and 4,4′-bipyridine, *Acta Crystallogr. C*, **75**, 723 (2019).
2. Z. Razmara, Lanthanum(III) complex as ferromagnetic supraprecursor for preparation of La_2O_3 nanoparticles by thermal decomposition method, *Res. Chem. Intermed*., **45**, 2887 (2019).
3. C. C. Zhang, S. Y. Wei, L. X. Sun, F. Xu, P. R. Huang and H. L. Peng, Synthesis, structure and photocatalysis properties of two 3D isostructural Ln(III)-MOFs based 2,6-pyridinedicarboxylic acid, *J. Mater. Sci. Technol.*, **34**, 1526 (2018).
4. T. Chuasaard, A. Ngamjarurojana, S. Surinwong, T. Konno, S. Bureekaew and A. Rujiwatra, Lanthanide coordination polymers of mixed phthalate/adipatefor ratiometric temperature sensing in the upper- intermediate temperature range, *Inorg. Chem.*, **57**, 2620 (2018).
5. P. Thuéry and J. Harrowfield, Ag^{I} and Pb^{II} as additional assembling cations in uranyl coordination polymers and frameworks, *Cryst. Growth Des.*, **17**, 2116 (2017).
6. Ž. Soldin, B. M. Kukovec, D. Matković-Čalogović and Z. Popović, Hydrogen-bonded frameworks of mercury(II) complexes with pyridinedicarboxylic acids, *Aust. J. Chem.*, **71**, 455 (2018).
7. X. L. Wang, C. Qin, E. B. Wang, C. W. Hu and L. Xu, A novel three-dimensional supramolecular network containing one-dimensional trapezoid channels based on nickel and mixed organic ligands assembly, *J. Mol. Struct*., **692**, 187 (2004).
8. C. J. He, L. L. Zang, W. Y. Wang and Y. F. Wang, Cadmium(II) and nickel(II) complexes with 4-hydroxypyridine-2,6-dicarboxylic acid: synthesis and crystal structures, *Synth. React. Inorg. Met.-Org. Nano-Met. Chem.*, **43**, 784 (2013).
9. S. Song, C. Y. Shao, H. M. Zhang, W. Zhang, L. R. Yang, T. G. Ren and Z. W. Bu, A 2D hydrogen-bonded 1D coordination network of Pr(III) with pyridine-2,6-dicarboxylic acid: hydrothermal synthesis, structure, and luminescent properties, *Synth. React. Inorg. Met.-Org. Nano-Met. Chem.*, **43**, 169 (2013).
10. Z. Razmara, Synthesis, characterization and magnetic properties of bi-metallic copper complex, as a precursor for the preparation of CuO nanoparticles and its application for removal of arsenic from water, *J. Inorg. Organomet. P.*, **28**, 1255 (2018).
11. S. Sharif, B. Khan, O. Şahin and I. U. Khan, Lanthanide complexes with pyridine-2,6-dicarboxylic acid: synthesis, crystal structure, thermal and magnetic properties of $[LnPDA)_2(PDAH_2)]\cdot(DMAH_2)_2(DMAH_{0.5})_2$, *Russ. J. Coord. Chem.*, **42**, 56 (2016).
12. Z. Derikvand, A. Azadbakht, B. Notash and E. Zamanifar, A new supramolecular coordination compound of Mg(II) with chelidamic acid; synthesis, spectroscopic, crystal structures and thermal analysis, *Inorg. Nano-Met. Chem.*, **47**, 515 (2017).
13. J. Soleimannejad, F. Moghzi, Sh. Hooshmand, Z. Dankoob, M. Ardalani and M. Shamsipur, A comparison of ligand behaviors and interactions during supramolecular assembly using molecular dynamics simulation: synthesis, solid state and solution studies of two Ni(II) compounds, *Polyhedron*, **133**, 24 (2017).
14. S. Abdolmaleki, M. Ghadermazi, M. Ashengroph, A. Saffari and S. M. Sabzkohi, Cobalt(II), zirconium(IV), calcium(II) complexes with dipicolinic acid and imidazole derivatives: X-ray studies, thermal analyses, evaluation as in vitro antibacterial and cytotoxic agents, *Inorg. Chim. Acta*, **480**, 70 (2018).
15. Z. A. Alkaya, H. İlkimen, C. Yenikaya, E. Tunca, M. Bülbül, T. Tunç and M. Sarı, Synthesis and characterization of Cu(II) complexes of 2-amino-6-sulfamoylbenzothiazole and their inhibition studies on carbonic anhydrase isoenzymes, *Polyhedron*, **151**, 199 (2018).
16. S. E. H. Etaiw, M. M. El-Bendary and H. Abdelazim, Synthesis, characterization, and biological activity of Cd(II) and Mn(II) coordination polymers based on pyridine-2,6-dicarboxylic acid, *Russ. J. Coord. Chem.*, **43**, 320 (2017).

17. G. Y. S. K. Swamy, P. Sivanarayanan, B. Sridhar and L. R. Joshi, Crystal structure studies and antimicrobial activities of transition metal complexes of pyridine-2,6-dicarboxylic acid and imidazole containing water clusters, *J. Coord. Chem.*, **69**, 1602 (2016).
18. I. A. Ansari, F. Sama, M. Shahid, Rahisuddin, R. Arif, M. Khalid and Z. A. Siddiqi, Isolation of proton transfer complexes containing 4-picolinium as cation and pyridine-2,6-dicarboxylate complex as anion: crystallographic and spectral investigations, antioxidant activities and molecular docking studies, *Rsc Adv.*, **6**, 11088 (2016).
19. L. L. Liu, X. S. Tai, J. B. Liu, D. Li, X. J. Zhou, L. J. Zhang and X. F. Wei, Preparation of propargylamines catalyzed by heterogeneous catalysts with double catalytic sites, *Chem. J. Chin. U.*, **39**, 482 (2018).
20. A. Karmakar, K. Deka, R. J. Sarma and J. B. Baruah, Benzoic acid inclusion in a dimeric nickel complex and its catalytic activity, *Inorg. Chem. Commun.*, **9**, 836 (2006).
21. D. Pyreu and S. Gridchin, Thermodynamics of mixed ligand complex formation of metal(II) iminodiacetates and nitrilotriacetates with dipyridyl and phenanthroline in solution, *J. Therm. Anal. Calorim.*, **139**, 1435 (2020).
22. Ö. Dağlı, D. A. Köse, O. İçten, G. A. Avcı and O. Şahin, The mixed ligand complexes of Co(II), Ni(II), Cu(II) and Zn(II) with coumarilic acid/1,10-phenanthroline, *J. Therm. Anal. Calorim.*, **136**, 1467 (2019).
23. G. Świderski, R. Świsłocka, R. Łyszczek, S. Wojtulewski, M. Samsonowicz and W. Lewandowski, Thermal, spectroscopic, X-ray and theoretical studies of metal complexes (sodium, manganese, copper, nickel, cobalt and zinc) with pyrimidine-5-carboxylic and pyrimidine-2-carboxylic acids, *J. Therm. Anal. Calorim.*, **138**, 2813 (2019).
24. B. B. Holló, L. S. V. Ješić, M. M. Radanović, M. V. Rodić, Ž. K. Jaćimović and K. M. Szécsényi, Synthesis, physicochemical, and thermal characterization of coordination compounds of Cu(II) with a pyrazole-type ligand, *J. Therm. Anal. Calorim.*, **142**, 451 (2020).
25. H. Wu, W. J. Sun, W. J. Zhao, T. Shi, X. Z. Liao and X. W. Yang, Self-penetrating and interpenetrating 3D metal–organic frameworks constructed from 4-(4-carboxyphenoxy)-phthalic acid and *N*-donor auxiliary ligands, *Chem. Pap.*, **69**, 300 (2015).
26. S. Demir, H. M. Çepni, M. Hołyńska, M. Kavanoz, F. Yilmaz and Y. Zorlu, Copper(II) complexes with pyridine-2,6-dicarboxylic acid from the oxidation of copper(I) iodide, *J. Coord. Chem.*, **70**, 3422 (2017).
27. H. Hadadzadeh, A. R. Rezvani, M. K. Abdolmaleki, K. Ghasemi, H. Esfandiari and M. Daryanavard, Pyridine-2,6-dicarboxylic acid (Dipic): crystal structure from co-crystal to a mixed ligand nickel(II) complex, *J. Chem. Crystallogr.*, **40**, 48 (2010).
28. N. G. Furmanova, Zh. I. Berdalieva, T. S. Chernaya, V. F. Resnyanskiĭ, N. K. Shiitieva and K. S. Sulaĭmankulov, Synthesis and crystal structures of coordination compounds of pyridoxine with zinc and cadmium sulfates, *Crystallogr. Rep.*, **54**, 228 (2009).
29. Q. Zang, G. Q. Zhong and M. L. Wang, A copper(II) complex with pyridine-2,6-dicarboxylic acid: Synthesis, characterization, thermal decomposition, bioactivity and interactions with herring sperm DNA, *Polyhedron*, **100**, 223 (2015).
30. M. J. Borah, R. K. B. Singh, U. B. Sinha, T. Swu and P. J. Borah, Synthesis and crystal structure determination of dimeric Co(II) and Ni(II) with pyridine 2,6-dicarboxylic acid, *J. Chem. Crystallogr.*, **42**, 67 (2012).
31. R. G. Yang, M. L. Wang, T. Liu T and G. Q. Zhong. Room temperature solid state synthesis, characterization, and application of a zinc complex with pyromellitic acid, *Crystals*, **8**, 56 (2018).
32. M. Mirzaei, H. Eshtiagh-Hosseini, Z. Karrabi, K. Molčanov, E. Eydizadeh, J. T. Mague, A. Bauzá and A. Frontera, Crystal engineering with coordination compounds of Ni^{II}, Co^{II}, and Cr^{III} bearing dipicolinic acid driven by the nature of the noncovalent interactions, *CrystEngComm*, **16**, 5352 (2014).
33. N. Okabe and N. Oya, Copper(II) and zinc(II) complexes of pyridine-2,6-dicarboxylic acid, *Acta Crystallogr. C*, **56**, 305 (2000).
34. J. M. Huang, L. F. Xu, C. Qian and X. Z. Chen, *N*-alkylation of ethylenediamine with alcohols catalyzed by CuO-NiO/γ-Al_2O_3, *Chem. Pap.*, **66**, 304 (2012).
35. P. V. F. de Sousa, A. F. de Oliveira, A. A. da Silva, B. G. Vaz and R. P. Lopes, Study of ciprofloxacin degradation by zero-valent copper nanoparticles, *Chem. Pap.*, **73**, 249 (2019).
36. Z. M. Khoshhesab and M. Sarfaraz, Preparation and characterization of NiO nanoparticles by chemical precipitation method, *Synth. React. Inorg. Met.-Org. Nano-Met. Chem.*, **40**, 700 (2010).
37. G. P. Kim, I. Nam, S. Park, J. Park and J. Yi, Preparation via an electrochemical method of graphene films coated on both sides with NiO

nanoparticles for use as high-performance lithium ion anodes, *Nanotechnology*, **24**, 475402 (2013).
38. A. G. Xiao, S. B. Zhou, C. G. Zuo, Y. B. Zhuan and X. Ding, Improved electrochemical performances of CuO nanotube array prepared via electrodeposition as anode for lithium ion battery, *Mater. Res. Bull.*, **70**, 795 (2015).
39. S. Ghamari, M. Ranjbar and M. Nabitabar, Preparation and characterization of nanopowder nickel oxide/ gadolinium-doped ceria via the sol-gel method by $NiLH_2$ precursor, *J. Sol-Gel Sci. Techn.*, **81**, 236 (2017).
40. D. Y. Han, H. Y. Yang, C. B. Shen, X. Zhou and F. H. Wang, Synthesis and size control of NiO nanoparticles by water-in-oil microemulsion, *Powder Technol.*, **147**, 113 (2004).
41. G. M. Sheldrick, A short history of SHELX, *Acta Crystallogr. A*, **64**, 112 (2008).
42. G. Q. Zhong and Q. Zhong. Solid–solid synthesis, characterization, thermal decomposition and antibacterial activities of zinc(II) and nickel(II) complexes of glycine–vanillin Schiff base ligand, *Green Chem. Lett. Rev.*, **7**, 236 (2014).
43. D. Li and G. Q. Zhong, Synthesis and crystal structure of the bioinorganic complex $[Sb(Hedta)]\cdot 2H_2O$, *Bioinorg. Chem. Appl.*, **2014**, 461605 (2014).
44. H. Luo, R. G. Yang, Z. H. Chen and G.Q. Zhong, Three bismuth(III) complexes constructed by *N*-containing heterocyclic carboxylic acids: synthesis, crystal structure and photocatalytic activity, *J. Solid State Chem.*, **300**, 122256 (2021).
45. A. R. Costa, T. I. de Menezes, R. R. Nascimento, P. N. M. dos Anjos, R. B. Viana, A. G. de Araujo Fernandes and R. L. S. R. Santos, Ruthenium(II) dimethylsulfoxide complex with pyrazole/dithiocarbazate ligand, *J. Therm. Anal. Calorim.*, **138**, 1683 (2019).
46. A. Majumder, V. Gramlich, G. M. Rosair, S. R. Batten, J. D. Masuda, M. S. E. Fallah, J. Ribas, J. P. Sutter, C. Desplanches and S. Mitra, Five new cobalt(II) and copper(II)-1,2,4,5-benzenetetracarboxylate supramolecular architectures: syntheses, structures, and magnetic properties, *Cryst. Growth Des.*, **6**, 2355 (2006).
47. G. Q. Zhong, J. Shen, Q. Y. Jiang and K. B. Yu, Synthesis and structural determination of a novel heterometallic complex $[Sb_2(edta)_2\text{-}\mu_4\text{-}Co(H_2O)_2]\cdot 5.15H_2O$, *Chin. J. Chem.*, **29**, 2650 (2011).
48. S. Demir, V. T. Yilmaz, B. Sariboga, O. Buyukgungor and J. Mrozinski, Metal(II) nicotinamide complexes containing succinato, succinate and succinic scid: synthesis, crystal structures, magnetic, thermal, antimicrobial and fluorescent properties, *J Inorg Organomet Polym*, **20**, 220 (2010).
49. V. T. Yilmaz, S. Demir, O. Andac and W. T. A. Harrison, Mixed-ligand metal succinate complexes with 1,10-phenanthroline and ethylenediamine: synthesis, characterization, spectroscopic and thermal studies. crystal structure of succinatocobalt(II) complex with phenanthroline, *J Coord Chem*, **55**, 863 (2002).
50. G. Q. Zhong, D. Li and Z. P. Zhang, Hydrothermal synthesis, crystal structure and magnetic property of a homodinuclear ternary coordination polymer of nickel(II), *Polyhedron*, **111**, 11 (2016).
51. Y. El-Sayed, M. Gaber, N. El-Wakeil, A. Abdelaziz and A. El-Nagar, Metal complexes of azo mesalamine drug: synthesis, characterization, and their application as an inhibitor of pathogenic fungi, *Appl Organometal Chem*, **35**, e6290 (2021).
52. M. Gaber, T. A. Fayed, M. N. El-Nahass, H. A. Diab and M. M. El-Gamil, Synthesis, spectroscopic characterization and biological evaluation of a novel chemosensor with different metal ions, *Appl Organometal Chem*, **33**, e5133 (2019).
53. J. I. Langford, A rapid method for analysing the breadths of diffraction and spectral lines using the Voigt function, *J. Appl. Cryst.*, **11**, 10 (1978).